Research Square

Preprints are preliminary reports that have not undergone peer review.
They should not be considered conclusive, used to inform clinical practice,
or referenced by the media as validated information.

Biosorption of nickel and cadmium using Pachira aquatica Aubl. peel Biochar

Talita L. S. Nascimento
Federal University of Rio Grande do Norte
Karine F. S. Oliveira
Federal University of Rio Grande do Norte
Joemil O. D. Junior
Federal University of Rio Grande do Norte
Alexandre S. Pimenta
Federal University of Rio Grande Do Norte – UFRN
Dulce M. A. Melo
Federal University of Rio Grande do Norte
Marcus A. F Melo
Federal University of Rio Grande do Norte
Renata Martins Braga (renatabraga.r@gmail.com)
Federal University of Rio Grande do Norte

Research Article

Keywords: Adsorption, Heavy metals removal, Biomass, Biosorbent, Wastewater treatment

Posted Date: May 19th, 2023

DOI: https://doi.org/10.21203/rs.3.rs-2938170/v1

License: This work is licensed under a Creative Commons Attribution 4.0 International License.
Read Full License

Abstract

Chemical contamination of the environment by heavy metals is becoming a serious problem in the worldwide due to increased human activities and industrial development. Therefore, researchers have been looking for alternatives to remediate these contaminants with economical and efficient technologies. This work aimed to value *Pachira aquatica* Aubl. fruit peels through the applicability of this material in the biosorption process for removal of Ni(II) and Cd(II) metal ions. Characterization of *Pachira aquatica* Aubl. fruit peel biochar (PAB) was performed through the proximate analysis, helium pycnometry, XRD, SEM, point of zero charges, zeta potential, and Boehm titration method. Design of experiment (DOE) was carried out, as well as kinetic, isotherm, and thermodynamic batch biosorption, and finally, column biosorption tests were performed. The PAB presents potential as a biosorbent due to its low amount of moisture, density similar to that of commercial activated carbons, neutral point of zero charges, porous, irregular, heterogeneous, and negative surface within the presence of functional groups capable of efficiently connecting with heavy metal. The biosorption equilibrium time was obtained at 300 min for both ions, following a pseudo second-order kinetic model and Langmuir isotherm model. The column tests presented an exhaust volume of 40.2 mg/L and 29.2 mg/L for Ni(II) and Cd(II), respectively. Thus, it is concluded that the PAB has the potential as a biosorbent for the removal of heavy, it leads to the valorization of this co-product and the reduction of environmental pollution.

1. Introduction

Chemical contamination of the environment by heavy metals is becoming increasingly serious worldwide due to human activities and industrial development (Rajeshkumar et al. 2018). Ni(II) and Cd(II), besides Pb(II), have been listed as priority pollutants by the US Environmental Protection Agency (EPA) and French Water Agency (He et al. 2018; Loiacono et al. 2018). Due to their potential carcinogenicity, high toxicity, even at low concentration, long residence times, bioaccumulation and their non-decomposition by chemical or biological processes (Ayangbenro and Babalola 2017; Jiang et al. 2017)

Therefore, environmental monitoring agencies set maximum permitted limits for heavy metals in the water to protect human health and the ecosystem. In Brazil, for instance, the CONAMA N°430/2011 (BRASIL 2011) establishes that wastewaters containing heavy metals such as Ni(II) and Cd(II) must present a maximum of 2.0 mg/L and 0.2 mg/L, respectively, to be discharged into water bodies. Considering that, the concentration of Ni(II) and Cd(II) in an industrial effluent can reach 183 mg/L and 63 mg/L, respectively (Pooja et al. 2021), it is essential to use advanced techniques that can remove heavy metals from wastewater.

The most widely used technologies for this purpose are chemical precipitation, membrane filtration, coagulation and flocculation, ion exchange, adsorption, and electrochemical treatment. The disadvantages of these methods are their insufficient selectivity, high operating costs, technical limitations when the pollutants concentrations are low, and the production of waste sludge containing heavy metal loads (Pap et al. 2017).

To circumvent the disadvantages of conventional processes and/or make these processes more sustainable and effective, the use of alternative raw materials, such as lignocellulosic materials, are being incorporated into wastewater treatment processes. The valorization of agricultural waste biomass is more environmentally friendly because allows the use of various plant materials of easy access, low cost, abundant in nature, effective for low concentration of pollutants, minimum generation of toxic sludge, and easy regenerations for reuse (Gupta Vinod Kumar, Nayak Arunima 2015; Salih and Ghosh 2017).

Biosorption is a treatment that allows the use of agro-industrial waste biomass, using lignocellulosic materials as biosorbents. These materials have some characteristics that include: the existence of different functional groups such as alcohols, ketones, carboxylic acids, and phenols, that are present in the pores and/or on the surface of the adsorbent and affect their reactivity; high carbon content, which gives the material ideal hydrophobic characteristics for removal of oils and hydrocarbons; and controlled apparent density, to avoid its sedimentation at the bottom (RUTHVEN 1985)

A study by Correia et al, (2022) (Correia et al. 2022) showed that *Pachira aquatica* Aubl. (PA), popularly known as *monguba, munguba, castanheira-do-Maranhão*, or *cacau selvagem*, has several characteristics cited as important for the biosorption process. *Monguba* is a fruit species that can be found from Southern Mexico to northern Brazil. Its fruits are similar to cocoa and the seeds have nutritional potential because they contain many proteins, lipids, and minerals, being widely studied as unconventional food plants (UFPs) (Silva et al. 2020). The seed is also applicable as a biological controller due to the ethanolic extract that composes them, the oil obtained from the seeds can be used as an antioxidant and in biofuel production, and the leaves can be consumed as medicinal herbs (Pantoja et al. 2020; Rodrigues et al. 2019). Although PA has several applications, the peels of its fruits, which have woody characteristics and represent a large volume of the fruit (72.13%), have no defined application, they are treated as residues (Camacho and Ayala 2018; Correia et al. 2022).

Given the search for the development of sustainable materials for wastewater treatment and the use of waste. This work aimed to evaluate the applicability of a biosorbent produced from the biochar of the *Pachira aquatica* Aubl. fruit peel, which is considered an agricultural waste biomass, for the biosorption process aiming at the removal of Ni(II) and Cd(II) metal ions in batch and fixed bed column.

2. Material and methods

2.1. Biosorbent preparation

The biosorbent used was obtained from the carbonization process of the fruit peel of *Paquira aquatica* Aubl. (PA). The PA fruits were collected from trees present in the city of Natal, Rio Grande do Norte, Brazil. After oven drying, the peels were ground in a mechanical grinder, followed by a carbonization process at 450°C for 4 hours in a muffle furnace. The biochar produced from the PA peel, called PAB in this study, was screened and the particle size of 0.3–1.0 mm was washed with deionized water, dried, and stored for later use as biosorbent.

2.2. Biosorbent characterization

The proximate Analysis was performed to identify the moisture (ASTM E871-82), ash (ASTM E1755-01), volatile matter (ASTM E872-85), and fixed carbon, determined according to the Eq. 1 below:

Fixed carbon % = 100 - (moisture + ash + volatile matter) % Eq. 1

The PAB true density was obtained by a helium pycnometer performed in an Accupyc 1.330 equipment from Micrometics. The crystal structure of PAB was determined by X-ray diffraction (XRD) performed in a diffractometer D8 ADVANCE from Bruker, using CuKα radiation, at 1.000 W, and the data were recorded from 5–70° (2θ). The morphology was examined through scanning electron microscopy (SEM) analysis performed in an SSX-550 from Shimadzu, at a voltage of 15 kV. The point of zero charges (pH_{pzc}) was determined by adding 0.15 g of PAB with 25.0 mL of 0.1 mol/L NaCl to several Erlenmeyer flasks. A range of initial pH (pH_0) values of the NaCl solutions was adjusted from 3.0 to 11.0 by adding HCl and NaOH and these were agitated at 150 rpm at room temperature. At the end of 24 hours, the pH final values (pH_f) were measured and the graphic pH_0 versus pH_f was plotted. The zeta potential was measured by ZetaPlus – Zeta potential analyzer da Brookhaven Instruments Corporation, in which particles of PAB were suspended in an aqueous medium of pH 7.0 at room temperature. Boehm titration method was performed to identify the functional groups on the PAB surface; the process occurred according to the method adapted by Moradi-Choghamarani et al. (2019) (Moradi-Choghamarani et al. 2019).

2.3. Biosorption tests

To perform the biosorption tests a stock solution containing the adsorbates was prepared through the dissolution of Ni(NO) .6H O (VETEC – 97%) and Cd(NO3)2.6H O (Dinâmica – 99%) in deionized water. A synthetic multi-element solution at 100 mg/L of Ni(II) and 100 mg/L of Cd(II) was obtained and from the dilution of this solution other concentrations were obtained when necessary.

2.3.1. Statistical design of experiment

The biosorption design of the experiment of biosorption using PAB was carried out with three independent variables: (1) Temperature, (2) biosorbent mass, and (3) adsorbate concentration, with 2 levels each and triplicate at the central point, totaling the performance of 11 experiments ($P^k = 2^3+3$), according to full factorial design (FFD) with three center points. The design of the experiment was conducted according to Table 1 and for regression and graphical analysis of the data, STATISTICA 7.0 software was used.

The Metal ion removal efficiency by biosorbent (%) was calculated by Eq. 2.

$$E\,(\%) = \frac{C_{ai} - C_{ai}^{*}}{C_{ai}} 100 \qquad \text{Eq. 2}$$

No qual: = Metal ion removal efficiency (%);C_{ai} = Initial concentration (mg/L); C_{af} = Residual concentration (mg/L).

Samples were filtered using paper filters and the residual concentration of the synthetic multi-element solution was determined by Atomic Absorption Spectroscopy (AAS) in a SHIMADZU AA-6300, flame mode equipped with an air acetylene burner, at a wavelength of 232.0 e 228.0 nm, for Ni (II) and Cd (II), respectively. The experiments were carried out in the incubator with orbital agitation TE-420 from Technal, using 25 mL of solution, at room temperature (25°C), constant agitation of 150 rpm, and pH 5.0.

Table 1
Experimental matrix of the full factorial design with three center points

Design	Run order	Coded levels				Uncoded levels		
		Independent variables				Independent variables		
		T	m	C		T	m	C
						(°C)	(g)	(mg/L)
Factorial design	1	-1	-1	-1	=	30	0.1	10
	2	+ 1	-1	-1	=	50	0.1	10
	3	-1	+ 1	-1	=	30	0.5	10
	4	+ 1	+ 1	-1	=	50	0.5	10
	5	-1	-1	+ 1	=	30	0.1	70
	6	+ 1	-1	+ 1	=	50	0.1	70
	7	-1	+ 1	+ 1	=	30	0.5	70
	8	+ 1	+ 1	+ 1	=	50	0.5	70
Central design	9	0	0	0	=	40	0.3	40
	10	0	0	0	=	40	0.3	40
	11	0	0	0	=	40	0.3	40

2.3.2. Batch biosorption

Batch biosorption experiments were conducted using the agitation shaker LT 600/1 from LimaTec to control agitation and temperature. Samples containing only the synthetic multi-element solution (PAB free), subjected to the same conditions of agitation, temperature, and concentrations, were analyzed in all experiments, to evaluate analytical interferences during the experiments, these samples were called blank. All experiments were conducted in triplicate.

Biosorption kinetics was conducted using 125 mL Erlenmeyer flasks containing 0.5 g of PAB and 25 mL of a synthetic multi-element solution of 70 mg/L. The samples were sealed and placed in the incubator

under constant conditions of agitation at 150 rpm, pH 5 a 30°C. Aliquots were taken at intervals of 5, 10, 15, 30, 45, 60, 90, 120, 150, 180, 240, 300, 360, 420 e 480 min.

Biosorption isotherms were conducted using 125 mL Erlenmeyer flasks containing 0.5 g of PAB and 25 mL of synthetic multi-element solution with concentrations of 10, 20, 30, 40, 50, 60, 70, 80, 90 e 100 mg/L, submitted to constant agitation (150 rpm) at 30°C, pH 5, during 180 min.

Biosorption thermodynamic was conducted during 180 min, using 0,5 g of PAB in 25 mL of synthetic multi-element solution with a concentration of de 20, 40, 60, 80 e 100 mg/L, under constant agitation (150 rpm) and pH 5, temperature of 30, 40, 50 e 60°C.

At the end of each biosorption experiment the samples were filtered using paper filters and the AAS determined concentrations of the residual adsorbate. Table S.1 (Supplementary material) presents the models and equations used to evaluate batch biosorption data.

2.3.3. Fixed-bed column biosorption

Column experiments were carried out in a glass column with an internal diameter of 1.5 cm and a length of 23.5 cm packed with PAB and a supporting layer of glass wool was fitted at the bottom and at the top of the column to support the packing. The synthetic multi-element solution com pH 5.0 was pumped into the column in descending flow using a peristaltic from Technal.

The biosorption tests in the fixed-bed column were performed by varying the height of fixed-bed biosorption and adsorbate initial concentration, totaling three tests. In the first test, a fixed-bed column biosorption height of 9.0 cm was used, and an adsorbate initial concentration of 100 mg/L, this column was called column A. In the second test, the adsorbate initial concentrations were maintained equal, but the fixed-bed column biosorption height increased to 12.0 cm, this column was called column B. Finally, in the third test was used a fixed-bed biosorption height of 12.0 cm and adsorbate initial concentrations of 45 mg/L, this column was called column C. The three tests were performed with the same flow rate (3 mL/min), and in triplicate.

For column A, aliquots with a volume of 15 mL were collected every 5 min until 1200 mL was obtained. Columns B and C were collected aliquots of 12 mL every 4 min until 1000 mL was obtained. The operational parameters of the column were calculated according to the equations described in Table S.2 (Supplementary material).

3. Results and Discussions

3.1. Bioadsorbent characterization

The low value found for PAB moisture (6.55%) is favorable to the biosorption process since high moisture contents materials have their adsorptive capacity reduced by the occupation of their pores by water molecules. The largest component of the PAB was the fixed carbon (Fig. 1), a result associated with the

decomposition of the lignocellulosic components present in the material, which is the biosorption process. The occurrence of volatilization and chemical degradation of some compounds in PAB has resulted in a reduction in the volatile content, with a consequent proportional increase in mineral elements, that is, an increase in ash and fixed carbon content.

The density and volume of the PAB were 1.7094 g/cm³ and 0.4787 cm³, respectively. According to Dune et al. (2022) (Dune et al. 2022), higher coal densities provide higher volumes of activity, which indicates better quality coal. Comparing the density of PAB with the density of other biosorbents, such as those produced from the coconut shell (0.49–0.68 g/cm³), PAB is a better alternative because its density is relatively higher. In addition, the PAB has a density similar to that of commercial activated carbons (2.0–2.1 g/cm³), validating its quality as a biosorbent, in this aspect (Essuah, E.Y., Buah and University 2019)

The analysis by XRD depicted in Fig. S.1 (Supplementary material) showed that the PAB presents a primordially amorphous structure with disordered plane characteristics of biochar, in which the absence of crystallinity is associated with the removal of holocellulose in the carbonization process.

The PAB micrographs (Fig. 2) allow the observation of pores of different shapes and sizes and the rough surface with the presence of porous channels from the plant cell wall structure of the precursor biomass. The formation of pores on the surface of biochar and the expansion of the diameter of existing pores are attributed to the carbonization process. In the image with an increase of 1000x, it is possible to notice more clearly the irregularity of the surface, as well as the difference between the size of the pore channels.

It can be inferred that the surface of the PAB is porous, irregular, and heterogeneous, these characteristics are favorable for the biosorption process of heavy metals in an aqueous solution, since the adsorbed components are concentrated on the external surface and the larger this external surface per unit solid mass, the more favorable the biosorption will be.

The point of zero charges pH (Fig. 3) for PAB was 7.6, that is, it is within the neutrality range (6.0–7.6), being able to perform cations and anions adsorption. It is known that when the pH of the solution is lower than the pH_{pcz}, the surface of the material becomes positive, therefore, it repels positively charged ions. And when the pH of the solution is higher than pH_{pcz}, the surface of the material has a negative charge, so it attracts positively charged ions (Agarwal et al. 2020). For that reason, the PAB favors the cations adsorption in wastewater with a pH greater than 7.6, such as textile industry and pig slaughterhouse wastewater (Gerhardt et al. 2018).

The mean value for the zeta potential of PAB was − 56.94 mV. The strongly negative result indicates that the PAB surface has an affinity with cations, in which there will be an increase in the electrostatic attraction force between the biosorbent and the adsorbates Cd(II) and Ni(II) (Xu et al. 2017). The negatives charges on the surface of the material are related to the types of functional groups that compose it, and these groups favor the cationic biosorption process as they keep the adsorbate inside the

pore, assisting in the formation of the complexes that increase the biosorption capacity of the material (Ayangbenro and Babalola 2017).

The presence of carboxylic groups (1.03 mmol/g), phenolic groups (0.57 mmol/g), and lactonic groups (0.57 mmol/g) were observed, which are functional groups capable of efficiently connecting with heavy metal, being favorable to the biosorption process. The presence of these groups was also observed on the PAB surface in the FTIR performed by Júnior et al. (2021) (Oliveira et al.), from the identification of bands 3725–3792 cm^{-1} related to axial deformations in the O-H group. Besides that, there were observed peaks at 3000–2700 cm^{-1}, 1800–1100 cm^{-1}, and 900–500 cm^{-1} related to the stretching of the C-H group, the vibration of C = C bond, and the deformation of C-H bond, respectively. These groups serve as potential sites for an efficient biosorption of cations confirmed by Patra et al. (2020) (Patra et al. 2020) who reported major changes in the intensities of band peaks before and after cation adsorption.

The basic surface and the formations of bands 1700–1600 cm^{-1} referring to the elongation vibration of C = O, identified in the FTIR performed by Júnior et al. (2021) (Oliveira et al.), are related to the presence of basic oxygenated functional groups, such as hydroxyl, carbonyl, and carboxyl groups. These groups are recognized as one of the main contributors to the arrangement between heavy metals and adsorbent surfaces, acting as active sites (Nartey and Zhao 2014). Moreover, the existence of negatively charged functional groups on the PAB surface indicates that compounds with a positive charge (cations) will be more easily absorbed by this material due to the electrostatic interaction that will occur between cations and anions (C. et al. 2019).

3.2. Adsorption tests

3.2.1. Statistical design of experiment

The Pareto chart, in Fig. S.2 (Supplementary material), shows in decreasing order of relevance, the effects of each factor and its interactions in the response variable. The factors related to the interaction of temperature with adsorbate concentration for Ni(II) removal and interactions of temperature and biosorbent mass for Cd (II) removal were insignificant to the process, indicating that for Ni(II) the adsorbate concentration and Cd(II), the biosorbent mass is independent of the temperature variation of the process. The adsorbate concentration was the factor that most affected the process, presenting negative effects. Therefore, the reduction of adsorbate concentration in the process will lead to greater removals of metal ions due to the higher amount of available binding sites.

From the contour plot (Fig. 4) is possible to observe that for all temperatures, the red band (which indicates removal > 80%) presented similar sizes in that the 100% removal interval, slightly large for T = 50°C. Among the beneficial effects of temperature increase is the decrease in the solution viscosity, which causes an increase in the adsorbate diffusion rate in the limit layer of the pores of the adsorbent. The possibility of pore clearance, allowing the penetration of larger adsorbate molecules; and the increase in the degree of agitation of adsorbate molecules, which allows greater contact with the biosorbent and promotes greater adsorption (Müller et al. 2019).

Comparing the surfaces of both ions, under the same temperature, it can be inferred that the biosorbent is more efficient for Cd(II) removal, since the areas referring to the removal range of 80–100% were higher for this ion, at all temperatures. Similar results were observed by Nascimento et al. (2021) (Nascimento et al. 2021) in their tests for biosorption of Ni(II) and Cd(II), besides Fe(II), in charcoal produced from the peels of *Pachira aquatica* Aubl. It is also observed that, for any fixed metal concentration, the increase in biosorbent mass generates an increase in the metal ion removal, this behavior was expected since the increase in the biosorbent amount increases the number of sites available for biosorption (Agarwal et al. 2020).

A linear mathematical model was obtained that correlates the independent variables with the removal of Ni(II) and Cd(II) through the biosorption process. The models are described by Eq. 3 and Eq. 4 for Ni(II) and Cd(II), respectively, and these were evaluated by ANOVA described in Table S.3 (Supplementary material) in which it can be affirmed that the calculated linear model is statistically significant for the study of Ni(II) and Cd(II) removal through the biosorption process using the PAB. In which $x_{T,}$ x_{mb}, and x_{ca}, refer to the values of (°C), biosorbent mass (g), and adsorbate concentration (mg/L), respectively:

$$\eta_{Ni}^{2+} = 0{,}370633 + 0{,}013825x_T + 0{,}931520x_{mb} - 0{,}012140x_{ca} - 0{,}016149x_T x_{mb} + 0{,}015882\, x_{mb}x_{ca} \quad \text{Eq. 3}$$

$$\eta_{Cd}^{2+} = 1{,}221062 - 0{,}018337\, x_{ca} + 0{,}000085\, x_T\, x_{ca} + 0{,}026567\, x_{mb}\, x_{ca} \quad \text{Eq. 4}$$

3.2.2. Adsorption Kinects

The results obtained for the kinetic biosorption, Fig. 5 (a), it was possible to observe that the biosorption process was slow and occurred continuously, taking about 300 min to reach equilibrium. At this point, the removal of the ions was 81% for Ni(II) and 96% for Cd(II), with the adsorbed amount (q_e) of 2.7 mg/g and 3.5 mg/g of Ni(II) and Cd(II), respectively, after 300 min there was still removal.

To investigate the rate and the controlling mechanism of the biosorption process, the pseudo first-order model, Fig. 5 (b), pseudo second-order model, Fig. 5 (c), and intraparticle diffusion linear and non-linear model, Fig. 5 (d), were used to fit the data. The parameters for each model are shown in Table 2.

In the pseudo first-order model, the values obtained for K_1 indicate that the metal concentration in the solution decreases with the contact time, which is consistent with the literature. Observing the metal amount adsorbed per gram of biosorbent in the equilibrium (q_e) of the analyzed models, it is possible to verify that the pseudo second-order model provided results closer to the experimental data, besides having R^2 greater than 0.99 for the two metal ions.

Applying the nonlinear intraparticle diffusion model is possible to verify, there is a significant improvement in the adjustment about the application of the same model, both linear and nonlinear, being evident with an increase in the value of R^2, but its increase is not yet ≥ 0.99.

The pseudo second-order model was the one that provided the best fit since it performed a data prediction closer to the experimental data [Fig. 6 (a) and (b)]. The equilibrium using the pseudo second-order model was achieved at 240 min, and such as for the experimental data, after 240 min there was still removal, but slower and with reduced values. According to Pal and Pal (2017) (Pal and Pal 2017), if the biosorption process follows the pseudo second-order model, the removal is assumed due to the physical-chemical interaction between the adsorbate and biosorbent, which involves the donation or sharing of electrons, from the covalent or ionic bonding forces. This model is recommended for a process that occurs in a longer period of biosorption, which occurred for biosorption with PAB (Agarwal et al. 2020). Moreover, the molecules in this type of biosorption are not attracted to the entire surface of the solid, but specifically by activated sites to initially form a monolayer, with the possibility of the formation of another layer by physisorption (Tural et al. 2016). The continuous behavior of kinetic curves suggests the occurrence of monolayer adsorption; this behavior is characteristic of the chemisorption processes.

Table 2
Adjustment parameters obtained from Pseudo first-order, Pseudo second-order, and Intraparticle diffusion models for the biosorption of the Ni(II) and Cd(II) metal ions.

Kinetic model	Parameters	Ni(II)	Cd(II)
Pseudo first-order	q_e(mg/g)	1,89	1,91
	K_1(min^{-1})	-0,0113	-0,0127
	R^2	0,931	0,968
Pseudo second-order	q_e(mg/g)	2,93	3,69
	K_2(min/g.mg^{-1})	0,0143	0,0192
	R^2	0,995	0,999
Intraparticle diffusion (Linear)	C (mg/g)	0,80	1,34
	K_d(min/g.$mg^{1/2}$)	0,1106	0,1277
	R^2	0,876	0,753
Intraparticle diffusion (Non-Linear)	C (mg/g)	0,63	0,77
	K_d(min/g.$mg^{1/2}$)	0,0662	0,4100
	R^2	0,988	0,934

3.2.3. Adsorption Isotherms

The biosorption isotherm profile, Fig. 7 (a), indicates that there is an increase in the biosorption capacity with the increase of adsorbate concentration, in which, the maximum concentration used (100 mg/L) for

Cd(II) provided greater biosorption capacity. For Ni(II) was until the concentration of 70 mg/L, because after this value the biosorption capacity becomes practically constant.

The concentration gradient, which becomes larger as the adsorbate concentration increases, promoted number of collisions between the biosorbent and the ions, causing a faster mass transport, due to an increase in the diffusion coefficient or mass transfer coefficient, consequently, the biosorption capacity will be higher (Chen et al. 2012; Long et al. 2014).

The equilibrium data isotherm was mathematically expressed in terms of biosorption isotherm models. The Langmuir model, Fig. 7 (b), and Freundlich model, Fig. 7 (c), were used and the parameters calculated for each model were shown in Table 3.

The maximum biosorption capacity given by the Langmuir model (q_{max}) e Freundlich model (K_f) show opposite results, in which for q_{max} the order of biosorption capacity of the PAB was Cd(II) > Ni(II) and for K_f Ni(II) > Cd(II). The experimental biosorption capacity followed the order presented by the Langmuir model. However, the order of the K_L, which is an indication of the Langmuir model for the affinity between the biosorbent surface and the adsorbate, is in accordance with the order presented by the Freundlich model. Such disagreement can be explained by the physical-chemical properties of metal ions.

Table 3
Adjustment parameters obtained from Langmuir and Freundlich models for the biosorption of the Ni(II) and Cd(II) metal ions.

Isotherm model	Parameters	Ni(II)	Cd(II)
Langmuir	**$q_{máx}$(mg/g)**	5,65	30,44
	K_L(L/g)	0,0109	0,0017
	R_L	0,48 – 0,90	0,86 – 0,98
	R^2	0,922	0,885
Freundlich	**N**	0,35	0,22
	1/n	2,84	4,48
	K_f*	0,00160	0,00001
	R^2	0,9627	0,8837
* $(mg.g^{-1})(L.mg^{-1})^{1/n}$			

According to Liu and Lian (2019) (Liu and Lian 2019), although Ni(II) has a greater affinity for the biosorbent surface due to its greater electronegativity, is proven by its higher value of *n* which represents the interaction force biosorbent/adsorbate, the largest ionic radius of Cd(II) can prevent Ni(II) access to

the pores of the biosorbent. Thus, the ionic radius is better applicable as an indicator of affinity between biosorbent surface and adsorbate comparing mononelementary systems where there are no ions dispute. From the evaluation of the parameters obtained for each model, it is possible to verify, mainly from the order of biosorption capacity, then Langmuir model promoted a better description of the experimental data, corroborating the modeling presented in Fig. 8.

In agreement with the Langmuir isotherm model, biosorption occurs in monolayer and metal uptake occurs on a homogeneous surface (Singh et al. 2020). The monolayer biosorption suggested by the Langmuir model confirms the results obtained for the biosorption kinetics described by the pseudo second-order model, indicating the occurrence of chemisorption.

3.2.4. Adsorption Thermodynamics

The thermodynamic parameters evaluated, in Table 4, demonstrate that the biosorption occurred in a way favorable and spontaneous (ΔG < 0), endothermic (ΔH >0), and with increased randomness of the system during sorption (ΔS > 0). Negative values for ΔG accompanied by positive values for ΔS indicate that the biosorbent has an affinity for the adsorbate.

The endothermic process explains the positive influence of temperature increase in the biosorption process using the PAB. In addition, the high values of ΔH revealed that chemisorption has occurred, as they are within the range 20,9–418,4 kJ/mol taken as the heat range of the chemisorption (Sari and Tuzen 2008). Ogbodu et al (2015) (R. O. Ogbodu, M. O. Omorogie, E. I. Unuabonah 2015) reported the occurrence of chemisorption in the biosorption process of Ni(II) and Cd(II) using Parkia biglobosa biomass in which the biosorption capacity followed the order indicated in this study [Cd(II) > Ni(II)].

Table 4
Thermodynamic parameters for the biosorption of the Ni(II) and Cd(II) metal ions.

Ions	Temperature	ΔG	ΔH	ΔS	R²
	°C	kJ/mol	kJ/mol	kJ/mol.K	
Ni(II)	30	-59,02	54,88	0,014	0,81
	40	-59,15			
	50	-59,29			
	60	-59,42			
Cd(II)	30	-124,69	119,83	0,034	0,72
	40	-124,85			
	50	-125,01			
	60	-125,17			

3.2.5. Fixed-bed column biosorption

The breakthrough of columns A, B, and C (Fig. 9) for Ni(II) and Cd(II) presents a slight asymmetrical S-shaped curve, characteristic of the ideal systems. Through the operational parameters of the column (Table 5) it is seen that the time to reach the exhaustion point (t_x) and the rupture point (t_b) was higher for column C, with consequently higher volumes of exhaustion (V_x) and rupture (V_b). This result is related to the bed depth increased from 9 cm to 12 cm, resulting in an increased amount of available binding sites for the column biosorption and increased contact time (Chen et al. 2012; Long et al. 2014). In addition, the reduction of adsorbate concentration from 100 gm/L to 45 mg/L decreased the driving forces for mass transfer, making the binding sites saturate more slowly (Mthombeni et al. 2018).

The C/C_0 ratio of both ions for all columns did not reach the unit value, then the total saturation of the biosorbent bed was not reached, but it came very close to this result. This can be confirmed by the percentage of positive saturation (%sat) of the columns.

The lengths of the mass transfer zone – MTZ (δ) obtained for the metal ions in the three columns were shorter than the length of the biosorbent bed. Comparing the results obtained, it can be seen that the shorter lengths of MTZ were achieved with column C for Ni(II) and with column B for Cd(II). The smaller the MTZ, the closer the system is to ideality. In view of this, the results show that there is competition between Ni(II) and Cd(II) ions for active sites, where, Cd(II) is favored, behavior recorded in different studies (Gadd 2009). However in lower concentrations, there is less competition due to greater availability of active sites, which allows the biosorption of higher amounts of Ni(II).

Table 5
Operational parameters in a fixed-bed column for Ni(II) and Cd(II) biosorption by PAB

Parameter	Column A		Column B		Column C	
	Ni(II)	Cd(II)	Ni(II)	Cd(II)	Ni(II)	Cd(II)
C/C_0Máx	0,98	0,98	0,94	0,99	0,86	0,95
t_b(min)	6,0	8,0	10,0	12,0	60	80
t_x(min)	300,0	60,0	320,0	80,0	400	360
V_b(mg/L)	18,0	24,0	30,0	36,0	180	240
V_x(mg/L)	900,0	180,0	960,0	240,0	1200	1080
δ (cm)	8,1	7,4	10,5	5,5	7,8	8,4
%sat	23,9	26,7	31,0	59,5	47,8	49,3

3.3. Mechanisms of Ni(II) and Cd(II) Biosorption by PAB

The results obtained in all experiments indicate that the PAB has good biosorption capacity for Ni(II) and Cd(II). The Boehm titration test and FTIR showed the presence of acid groups -OH and -COOH on the surface of the PAB. The presence of these groups indicates the occurrence of cation biosorption from the complexion mechanism (Nartey and Zhao 2014). Besides, the presence of basic groups in predominance and groups with a negative surface, point to the occurrence of electrostatic interaction and ion exchange between the PAB surface and cations, whose ion exchange occurs between cations and light bivalent metals, such as Ca(II) and Mg(II), found on the surface of biosorbents from lignocellulosic waste materials (Krishnani 2016).

According to Chao and Chang (2012), if the ion exchange is the primary mechanism of biosorption, the biosorption capacities of the heavy metals must be proportional to the ionic radius, in which, Ni(II) has a relatively higher potential to form complexes and the Cd(II) generates higher biosorption amounts through ion exchange (Chao and Chang 2012). In the present study, the order of adsorption capacities was proportional to the ionic radius and the highest biosorption capacity was for Cd(II) indicating ion exchange as the main mechanism. Given the above, three Biosorption mechanisms were proposed for Ni(II) and Cd(II) removal: Ion exchange, complexation, and electrostatic interaction (Fig. 10)

4. Conclusions

According to the present results, the PAB has the potential as a biosorbent of Ni(II) and Cd(II) due to its characteristics of high porosity, presence of functional groups, and bond groups, which favor the biosorption, and negative charge of its surface, that promotes electrostatic attraction and ion exchange with cations. The results of the batch biosorption tests showed that the process occurred slowly, continuously, and in monolayers. The interaction between the PAB and biosorbent occurred via chemisorption, and the main mechanisms involved in the process were ion exchange, complexation, and electrostatic attraction. The column biosorption showed that the biosorption capacity was higher for the Cd(II) than the Ni(II), but using lower initial concentrations (45 mg/L), higher amounts of Ni(II) were removed indicating that there was competition for binding sites, in which Cd(II) was favored due to its higher ionic radius. Thus, it is concluded that the PAB has the potential to remove heavy metals in the process of biosorption in batch process and fixed bed columns. There is also the possibility of applying the PAB as part of a combined process and/or tertiary treatment. All the applications lead to the valorization of this residue that has no defined applications, the reduction of solid waste, then the reduction of environmental pollution.

Declarations

Acknowledgements

This research was supported by the Brazilian National Council of Technological and Scientific Development (CNPq) - Project codes: 307433/2020-0, 311963/2021-8 - and Coordenação de

Aperfeiçoamento de Pessoal de Nível Superior - Brazil (CAPES). The authors are grateful to the LABTAM/NUPPRAR and UFRN for all the support for the development of this research.

Author contributions

Talita Lorena da Silva do Nascimento: Conceptualization, Writing - review & editing, Writing - original draft, Methodology, Data curation. **Karine Fonseca Soares de Oliveira:** Conceptualization, Methodology, Review. **Joemil Oliveira de Deus Junior:** Methodology, Data curation. **Alexandre Santos Pimenta:** Methodology. **Dulce Maria de Araújo Melo:** Supervision, Funding acquisition. **Marcus Antonio de Freitas Melo:** Conceptualization, Supervision. **Renata Martins Braga:** Conceptualization, Funding acquisition, Supervision.

Data Availability

Experimental data can be available from corresponding authors on reasonable request.

Ethical Approval: No applicable.

Funding: This research was supported financial from Coordenação de Aperfeiçoamento de Pessoal de Nível Superior - Brazil (CAPES).

Conflict of interest: The authors declare that they have no known competing financial interests or personal relationships that could have appeared to influence the work reported in this paper.

References

1. Agarwal, A., Upadhyay, U., Sreedhar, I., Singh, S.A., Patel, C.M.: A review on valorization of biomass in heavy metal removal from wastewater, (2020)
2. Ayangbenro, A.S., Babalola, O.O.: A new strategy for heavy metal polluted environments: A review of microbial biosorbents, www.mdpi.com/journal/ijerph, (2017)
3. BRASIL: CONAMA. Dispõe sobre as condições e padrões de lançamento de efluentes, complementa e altera a Resolução n. 357, de 17 de março de 2005. Resolução n. 430, de 13 de maio de 2011.
4. C., Lima, L.YASSUE-CORDEIRO, P.H., L., G., Pereira: Performance Analysis of Different Activated Carbons for the Effective Removal of HMF from Syrup Glucose. Rev. Virtual Química. 11, 909–921 (2019). https://doi.org/10.21577/1984-6835.20190063
5. Camacho, M.E., Ayala, C.C.: Correlations and path analysis between fruit characteristics and seeds of Pachira aquatica Aubl. Rev. Fac. Nac. Agron. Medellín. 71, 8387–8394 (2018). https://doi.org/10.15446/rfna.v71n1.67027
6. Chao, H.P., Chang, C.C.: Adsorption of copper(II), cadmium(II), nickel(II) and lead(II) from aqueous solution using biosorbents. Adsorption. 18, 395–401 (2012). https://doi.org/10.1007/s10450-012-9418-y

7. Chen, S., Yue, Q., Gao, B., Li, Q., Xu, X., Fu, K.: Adsorption of hexavalent chromium from aqueous solution by modified corn stalk: A fixed-bed column study. Bioresour. Technol. 113, 114–120 (2012). https://doi.org/10.1016/j.biortech.2011.11.110
8. Correia, L.A. da S., da Silva, J.E., Calixto, G.Q., Melo, D.M. de A., Braga, R.M.: Pachira aquatica fruits shells valorization: Renewables phenolics through analytical pyrolysis study (Py-GC/MS). Cienc. Rural. 52, 1–11 (2022). https://doi.org/10.1590/0103-8478CR20210068
9. Dune, K.K., Ademiluyi, F.T., Nmegbu, G.C.J., Dagde, K., Nwosi-Anele, A.S.: Production, Activation and Characterisation of PKS-Biochar from Elaeis Guineensis Biomass activated with HCl for Optimum Produced Water Treatment. Int. J. Recent Eng. Sci. 9, 1–7 (2022). https://doi.org/10.14445/23497157/ijres-v9i1p101
10. Essuah, E.Y., Buah, W.K., University: Effects of Steam Dosage on the Qualities of Activated Carbon Developed From Coconut Shells in Ghana. Int. J. Min. Sci. 5, 22–29 (2019). https://doi.org/10.20431/2454-9460.0504002
11. Gadd, G.M.: Biosorption: Critical review of scientific rationale, environmental importance and significance for pollution treatment. J. Chem. Technol. Biotechnol. 84, 13–28 (2009). https://doi.org/10.1002/jctb.1999
12. Gerhardt, R., Reisdorfer, G., Cardoso, M.G.: Remoção de nitrogênio e fósforo de efluente industrial através da precipitação de estruvita. TECNO-LÓGICA. 22, 35–40 (2018). https://doi.org/10.17058/tecnolog.v22i1.8858
13. Gupta Vinod Kumar, Nayak Arunima, S.A.: Bioadsorbents for remediation of heavy metals: Current status and their future prospects. Environ. Eng. Res. 20, 1–18 (2015). https://doi.org/10.4491/eer.2015.018
14. He, S., Li, Y., Weng, L., Wang, J., He, J., Liu, Y., Zhang, K., Wu, Q., Zhang, Y., Zhang, Z.: Competitive adsorption of Cd2+, Pb2+ and Ni2+ onto Fe3+-modified argillaceous limestone: Influence of pH, ionic strength and natural organic matters. Sci. Total Environ. 637–638, 69–78 (2018). https://doi.org/10.1016/j.scitotenv.2018.04.300
15. Jiang, Y., Chao, S., Liu, J., Yang, Y., Chen, Y., Zhang, A., Cao, H.: Source apportionment and health risk assessment of heavy metals in soil for a township in Jiangsu Province, China. Chemosphere. 168, 1658–1668 (2017). https://doi.org/10.1016/j.chemosphere.2016.11.088
16. Krishnani, K.K.: Lignocellulosic Wheat Straw-Derived Ion-Exchange Adsorbent for Heavy Metals Removal. Appl. Biochem. Biotechnol. 178, 670–686 (2016). https://doi.org/10.1007/s12010-015-1901-y
17. Liu, R., Lian, B.: Non-competitive and competitive adsorption of Cd2+, Ni2+, and Cu2+ by biogenic vaterite. Sci. Total Environ. 659, 122–130 (2019). https://doi.org/10.1016/j.scitotenv.2018.12.199
18. Loiacono, S., Crini, G., Chanet, G., Raschetti, M., Placet, V., Morin-Crini, N.: Metals in aqueous solutions and real effluents: biosorption behavior of a hemp-based felt. J. Chem. Technol. Biotechnol. 93, 2592–2601 (2018). https://doi.org/10.1002/jctb.5612

19. Long, Y., Lei, D., Ni, J., Ren, Z., Chen, C., Xu, H.: Packed bed column studies on lead(II) removal from industrial wastewater by modified Agaricus bisporus. Bioresour. Technol. 152, 457–463 (2014). https://doi.org/10.1016/j.biortech.2013.11.039
20. Moradi-Choghamarani, F., Moosavi, A.A., Baghernejad, M.: Determining organo-chemical composition of sugarcane bagasse-derived biochar as a function of pyrolysis temperature using proximate and Fourier transform infrared analyses. J. Therm. Anal. Calorim. 138, 331–342 (2019). https://doi.org/10.1007/s10973-019-08186-9
21. Mthombeni, N.H., Mbakop, S., Ray, S.C., Leswifi, T., Ochieng, A., Onyango, M.S.: Highly efficient removal of chromium (VI) through adsorption and reduction: A column dynamic study using magnetized natural zeolite-polypyrrole composite. J. Environ. Chem. Eng. 6, 4008–4017 (2018). https://doi.org/10.1016/j.jece.2018.05.038
22. Müller, L.C., De Almeida Alves, A.A., Mondardo, R.I., Sens, M.L.: Methylene blue adsorption in Pinus Elliottii (Pine) and drepanostachyum falcatum (bamboo) sawdust. Eng. Sanit. e Ambient. 24, 687–695 (2019). https://doi.org/10.1590/s1413-41522019160344
23. Nartey, O.D., Zhao, B.: Biochar preparation, characterization, and adsorptive capacity and its effect on bioavailability of contaminants: An overview. Adv. Mater. Sci. Eng. 2014, (2014). https://doi.org/10.1155/2014/715398
24. Nascimento, T.L. da S. do, Oliveira, K.F.S. de, Deus Junior, J.O. de, Melo, D.M. de A., Pimenta, A.S., Melo, M.A. de F., Braga, R.M.: Estudo dos fatores influentes no processo de biossorção em batelada de Fe3+, Ni2+ e Cd2+ utilizando bioadsorvente derivado da Pachira aquatica Aubl. Res. Soc. Dev. 10, e155101220321 (2021). https://doi.org/10.33448/rsd-v10i12.20321
25. Oliveira, J., Junior, D.D., Fonseca, K., Oliveira, S. De, Nascimento, T.L. da S. do, Braga, R.M.: Estudo cinético da remoção de íons metálicos de efluente aquoso utilizando finos de carvão provenientes da Pachira Aquatica Aubl .
26. Pal, P., Pal, A.: Surfactant-modified chitosan beads for cadmium ion adsorption. Int. J. Biol. Macromol. 104, 1548–1555 (2017). https://doi.org/10.1016/j.ijbiomac.2017.02.042
27. Pantoja, G.F., Cordeiro, Y.E.M., Silva, S.G., De Sousa, R.L.: Uso e aplicações medicinais da mamorana (Pachira aquatica Aublet) pelos ribeirinhos de São Lourenço, Igarapé-Miri, estado do Pará, Amazônia. Interações (Campo Gd. 21, 647–662 (2020). https://doi.org/10.20435/inter.v21i3.2146
28. Pap, S., Šolević Knudsen, T., Radonić, J., Maletić, S., Igić, S.M., Turk Sekulić, M.: Utilization of fruit processing industry waste as green activated carbon for the treatment of heavy metals and chlorophenols contaminated water. J. Clean. Prod. 162, 958–972 (2017). https://doi.org/10.1016/j.jclepro.2017.06.083
29. Patra, C., Shahnaz, T., Subbiah, S., Narayanasamy, S.: Comparative assessment of raw and acid-activated preparations of novel Pongamia pinnata shells for adsorption of hexavalent chromium from simulated wastewater. Environ. Sci. Pollut. Res. 27, 14836–14851 (2020). https://doi.org/10.1007/s11356-020-07979-y

30. Pooja, G., Kumar, P.S., Prasannamedha, G., Varjani, S., Vo, D.V.N.: Sustainable approach on removal of toxic metals from electroplating industrial wastewater using dissolved air flotation. J. Environ. Manage. 295, 113147 (2021). https://doi.org/10.1016/j.jenvman.2021.113147
31. R. O. Ogbodu, M. O. Omorogie, E. I. Unuabonah, J.O.B.: Biosorption of Heavy Metals from Aqueous Solutions by Parkia biglobosa Biomass: Equilibrium, Kinetics, and Thermodynamic Studies. Environ. Prog. Sustain. Energy. 34, 1694–1704 (2015). https://doi.org/10.1002/ep
32. Rajeshkumar, S., Liu, Y., Zhang, X., Ravikumar, B., Bai, G., Li, X.: Studies on seasonal pollution of heavy metals in water, sediment, fish and oyster from the Meiliang Bay of Taihu Lake in China. Chemosphere. 191, 626–638 (2018). https://doi.org/10.1016/j.chemosphere.2017.10.078
33. Rodrigues, A.P., Pereira, G.A., Tomé, P.H.F., Arruda, H.S., Eberlin, M.N., Pastore, G.M.: Chemical Composition and Antioxidant Activity of Monguba (Pachira aquatica) Seeds. Food Res. Int. 121, 880–887 (2019). https://doi.org/10.1016/j.foodres.2019.01.014
34. RUTHVEN, D.M.: Principles of adsorption and adsorption processes. John Wiley & Sons, New York (1985)
35. Salih, S.S., Ghosh, T.K.: Preparation and characterization of bioadsorbent beads for chromium and zinc ions adsorption. Cogent Environ. Sci. 3, (2017). https://doi.org/10.1080/23311843.2017.1401577
36. Sari, A., Tuzen, M.: Biosorption of cadmium(II) from aqueous solution by red algae (Ceramium virgatum): Equilibrium, kinetic and thermodynamic studies. J. Hazard. Mater. 157, 448–454 (2008). https://doi.org/10.1016/j.jhazmat.2008.01.008
37. Silva, T.G., Kasemodel, M.G.C., Ferreira, O.M., da Silva, R.C.L., Souza, C.J.F., Sanjinez-Argandona, E.J.: Addition of Pachira aquatica oil and Platonia insignis almond in cookies: Physicochemical and sensorial aspects. Food Sci. Nutr. 8, 5267–5274 (2020). https://doi.org/10.1002/fsn3.1368
38. Singh, S., Kumar, V., Datta, S., Dhanjal, D.S., Sharma, K., Samuel, J., Singh, J.: Current advancement and future prospect of biosorbents for bioremediation. Sci. Total Environ. 709, 135895 (2020). https://doi.org/10.1016/j.scitotenv.2019.135895
39. Tural, S., Tarhan, T., Tural, B.: Removal of hazardous azo dye Metanil Yellow from aqueous solution by cross-linked magnetic biosorbent; equilibrium and kinetic studies. Desalin. Water Treat. 57, 13347–13356 (2016). https://doi.org/10.1080/19443994.2015.1056842
40. Xu, L., Zheng, X., Cui, H., Zhu, Z., Liang, J., Zhou, J.: Equilibrium, Kinetic, and Thermodynamic Studies on the Adsorption of Cadmium from Aqueous Solution by Modified Biomass Ash. Bioinorg. Chem. Appl. 2017, (2017). https://doi.org/10.1155/2017/3695604

Figures

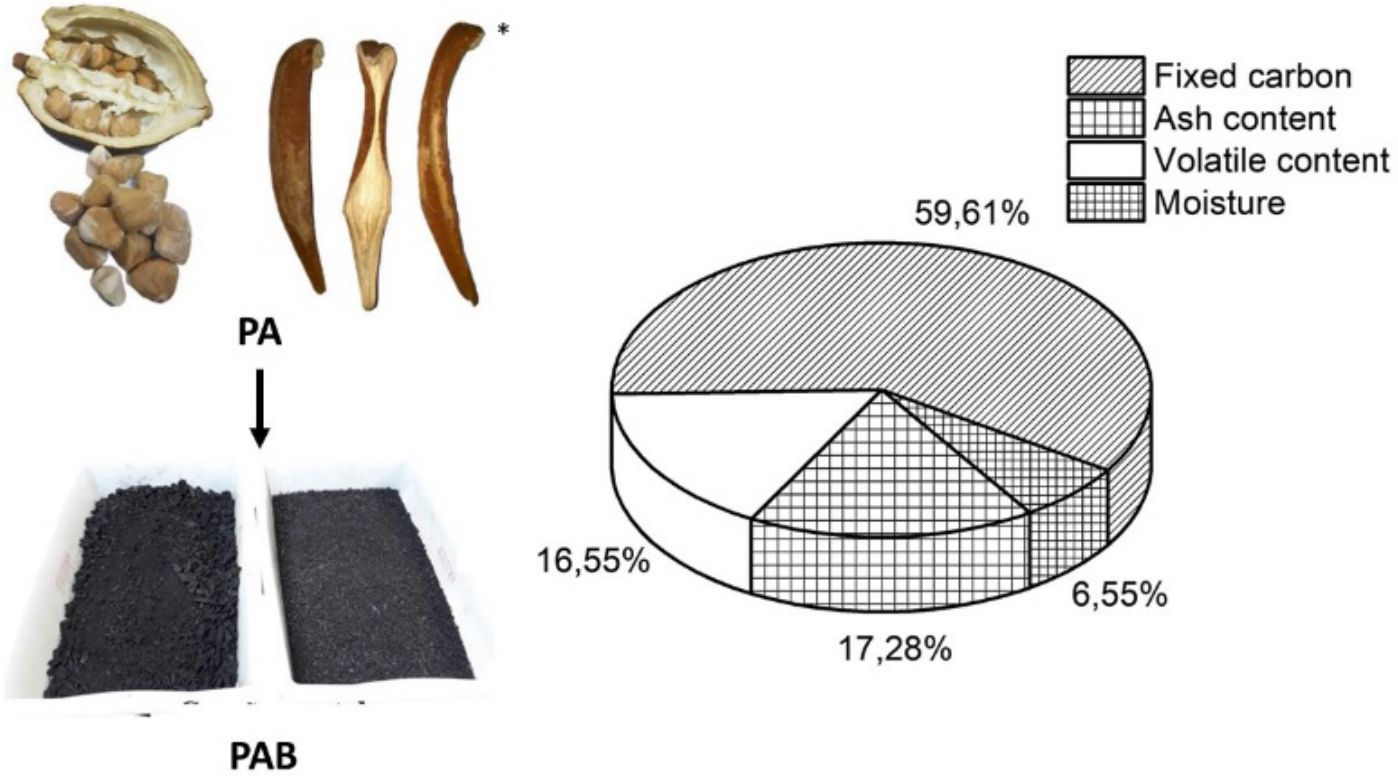

Figure 1

Immediate analysis results of PAB

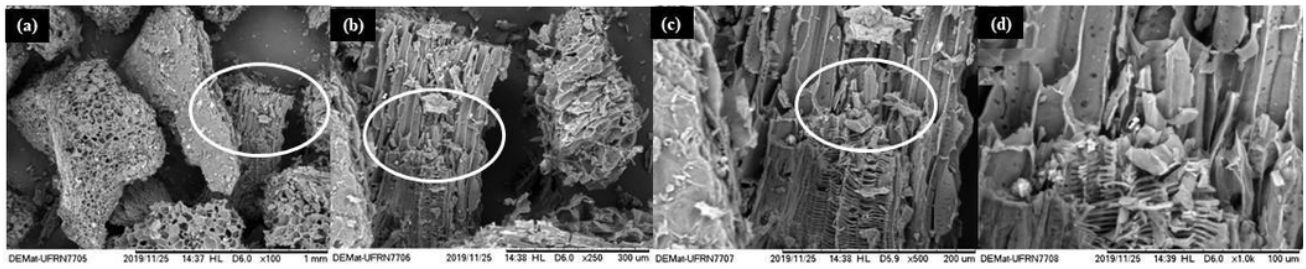

Figure 2

SEM images of the PAB in magnification of (a) 100, (b) 250, (c) 500 E (d) 1000 times

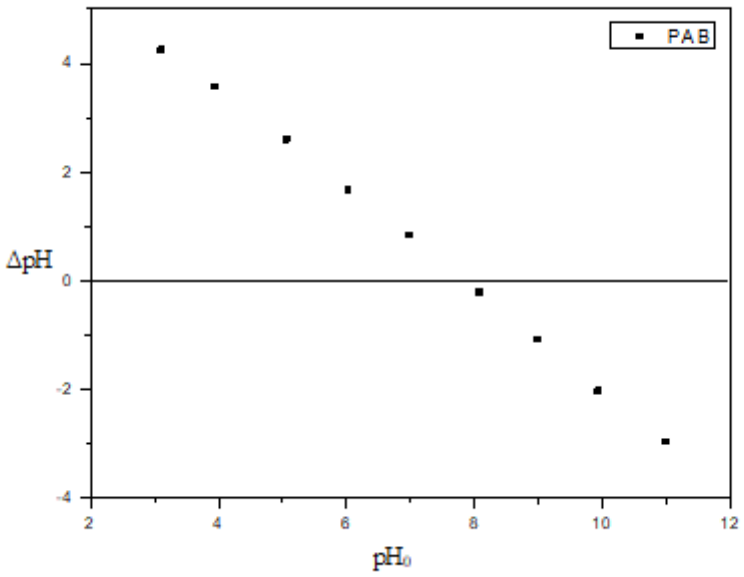

Figure 3

pH at point of zero charges (pH_{pcz}) of the PAB

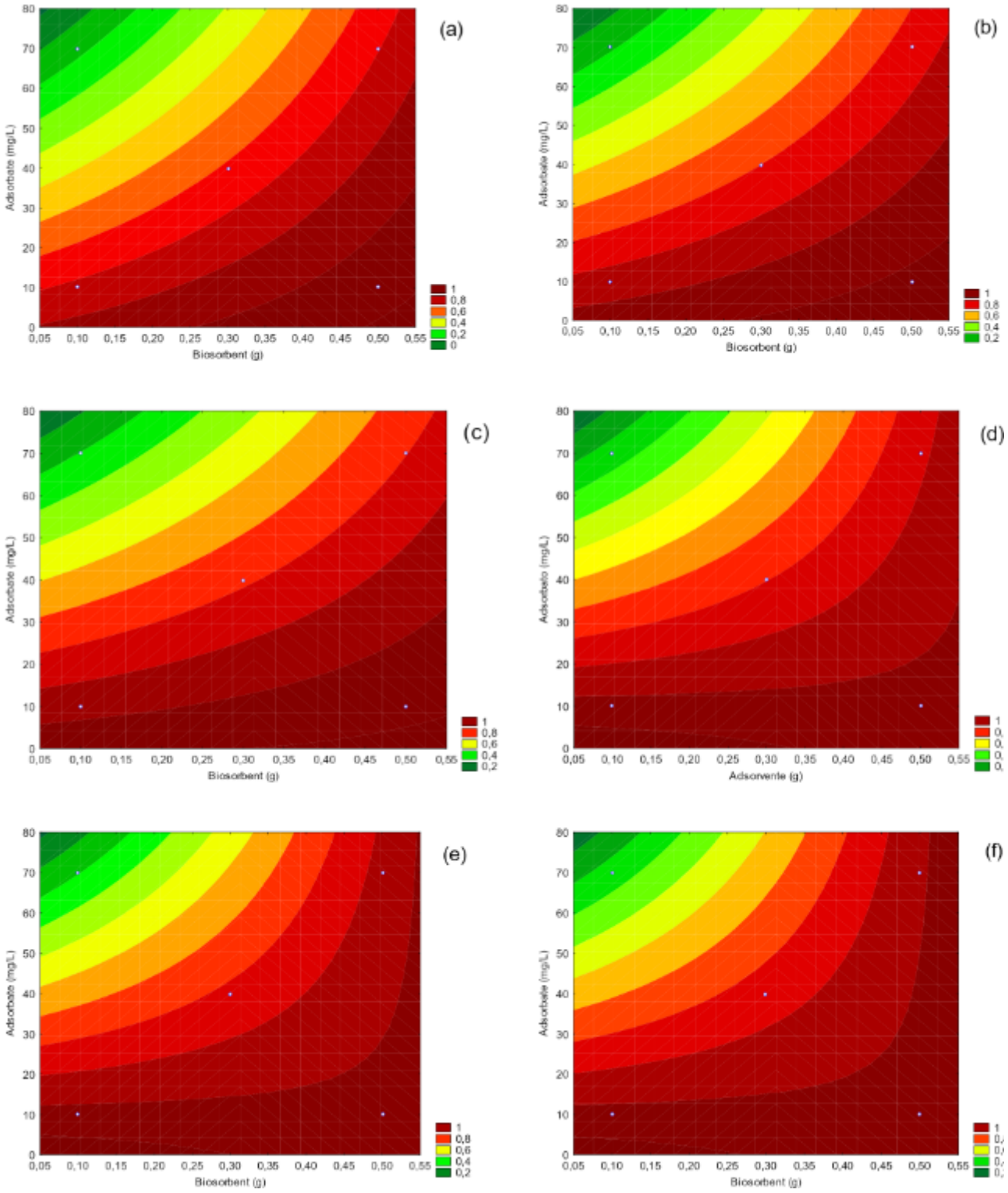

Figure 4

Contour plot for removal efficiency of Ni(II) in 3 temperatures: (a) T=30 °C, (b) T=40 °C e (c) T=50 °C and Cd(II) in three temperatures: (d) T=30 °C, (e) T=40 °C e (f) T=50 °C

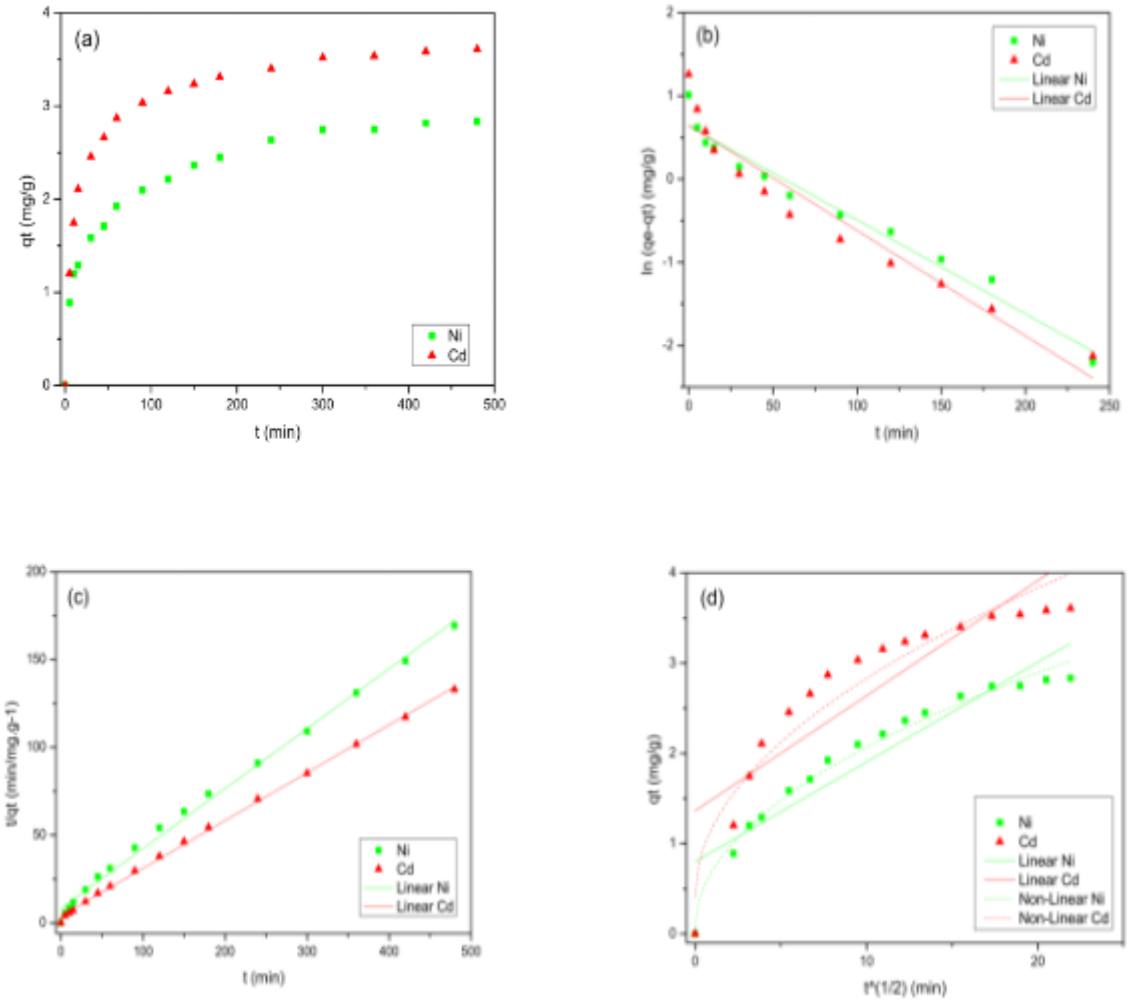

Figure 5

(a) Biosorption Kinetic of the Ni(II) e Cd(II) metal ions using the PAB biosorbent and Kinetics models of (b) Pseudo first-order, (c) Pseudo second-order and (d) Intraparticle diffusion linear and non-linear

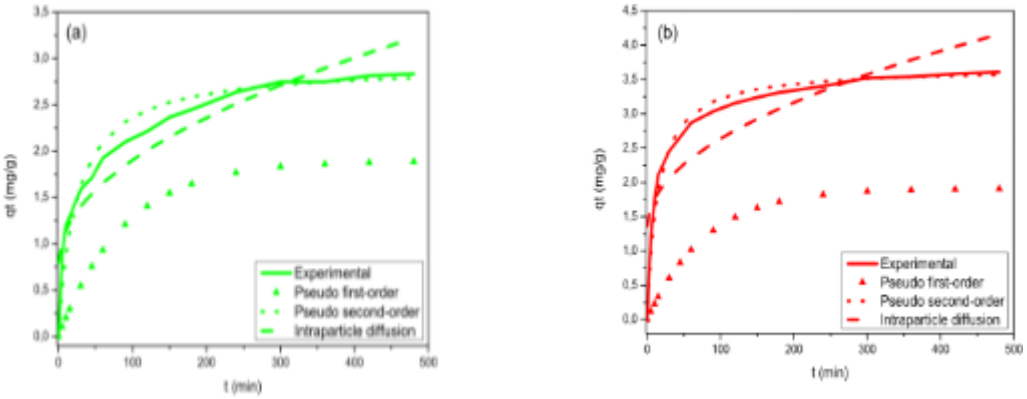

Figure 6

Biosorption kinetic results with experimental and calculated data according to Pseudo first-order, Pseudo second-order, and Intraparticle diffusion linear models for the biosorption of the (a) Ni(II) and (b) Cd(II) metal ion

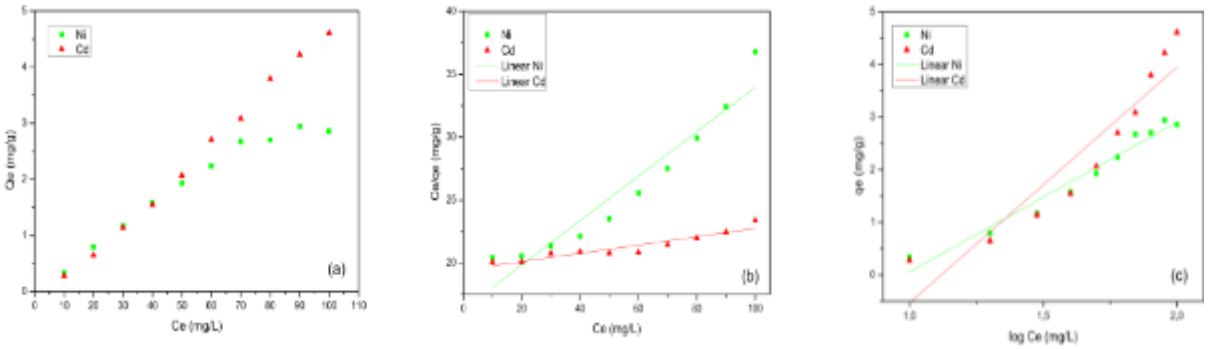

Figure 7

(a) Biosorption isotherms of the Ni(II) e Cd(II) metal ions using the PAB biosorbent and Isotherm models of (b) Langmuir and (c) Freundlich.

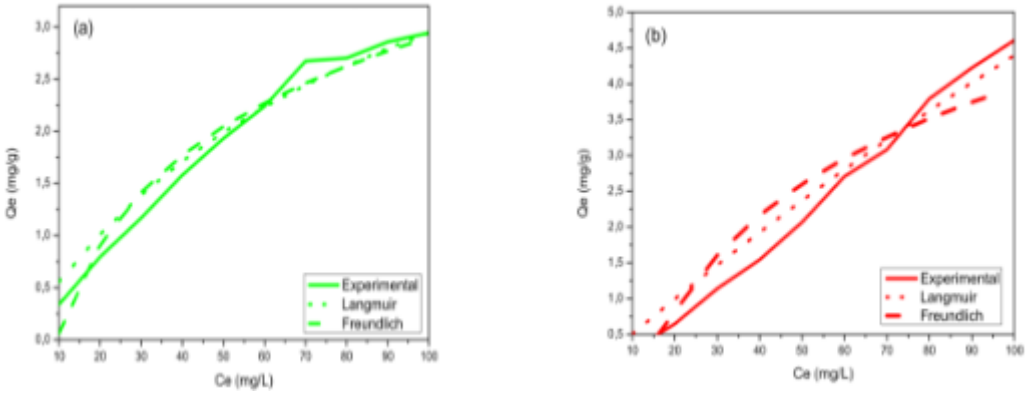

Figure 8

Biosorption isotherm results with experimental and calculated data according to Langmuir and Freundlich models for the biosorption of the (a) Ni(II) and (b) Cd(II) metal ion.

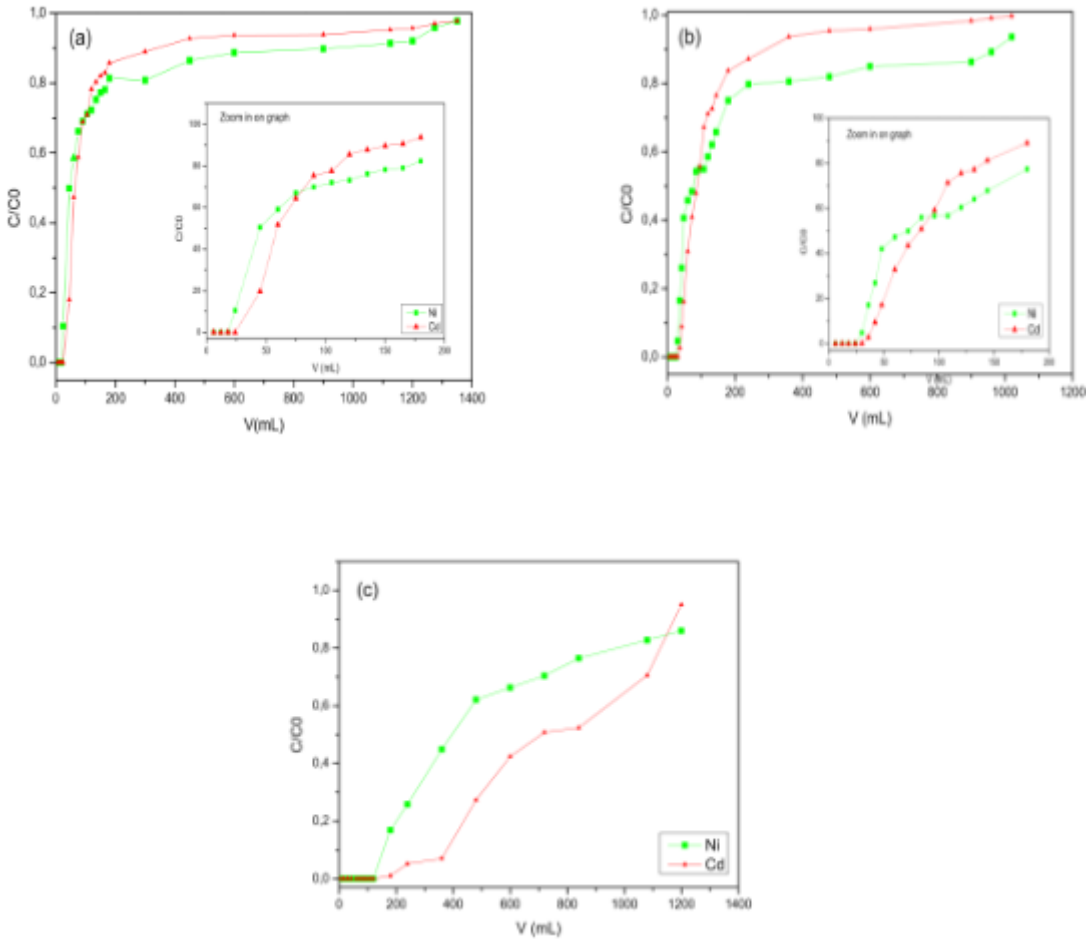

Figure 9

(a) Column A with 9 cm and concentration of 100 mg/L, (b) Column B with 12 cm and concentration of 100 mg/L, and (c) column C with 12 cm and concentration of 45 mg/L

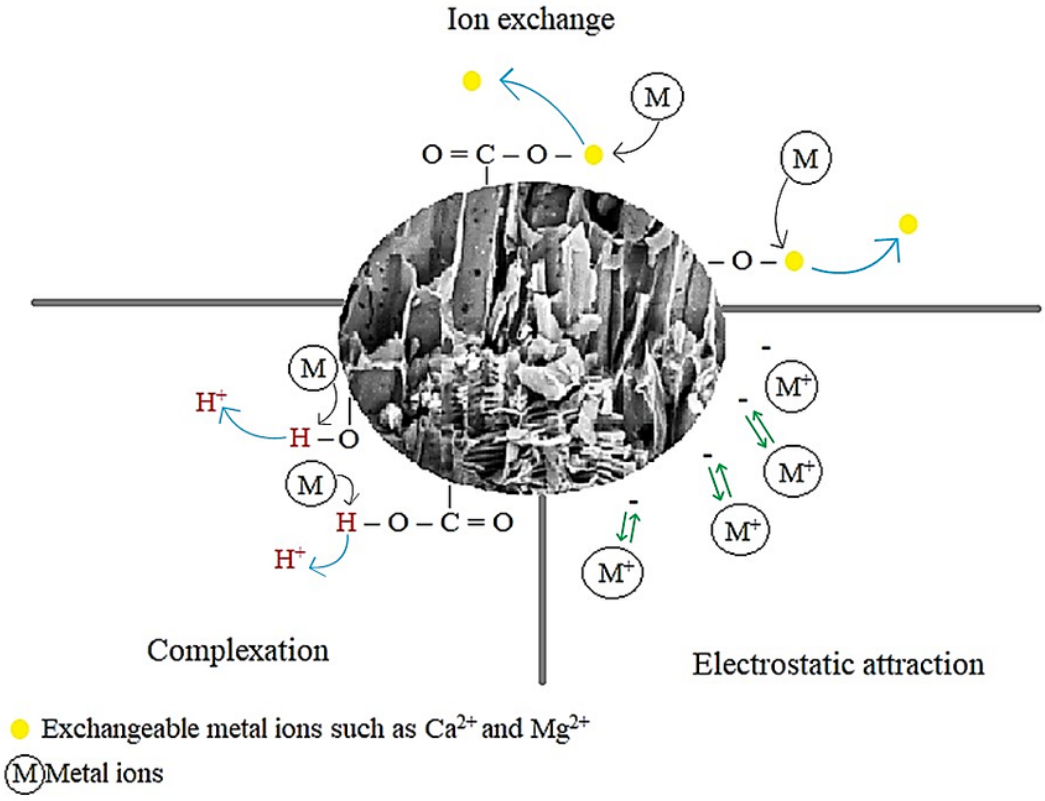

Figure 10

Illustration of heavy metal biosorption mechanisms on PAB

Supplementary Files

This is a list of supplementary files associated with this preprint. Click to download.

- GraphicalabstractPachira.docx
- SupplementaryMaterialPachira.docx